

ROOM TEMPERATURE FORMABILITY OF

ALLOYS 625LCF™, 718 AND 718SPF™

P. Roamer¹, C.J. Van Tyne, D.K. Matlock, A.M. Meier, H. Ruble² and F. Suarez²

Advanced Steel Processing and Products Research Center
Colorado School of Mines
Golden, CO 80401

¹Howmet Corporation
Dover Casting
Dover, NJ 07801

²INCO Alloys International
Huntington, WV 25720

Abstract

The formability of nickel-based alloys 625LCF, 718, and 718SPF is the focus of this study. Forming limit diagrams (FLD's) were constructed from limiting strain-ratio data. The formability behavior can be correlated to the mechanical properties and the failure mode of each alloy. The performance on the draw side of the forming limit diagram and at plane strain is controlled by the nickel-based matrix. On the draw side, the behavior agrees well with the uniaxial total elongation. The formability during biaxial stretching is controlled by inclusions and the fracture properties of the individual alloy. In general, the alloys studied have excellent formability especially if the particle content and particle size are controlled. However, these alloys are formable only with high loads compared to low carbon sheet steels.

Introduction

To enhance the desirable performance characteristics of superalloys considerable research has been applied to understanding their behavior during service. However, less attention has been paid to formability issues, especially to the sheet forming of these alloys. The high strength and strain-hardening behavior of nickel-base superalloys equate to high forming loads for room temperature fabrication which may cause manufacturing difficulties. The forming problems associated with these alloys, combined with the complex shapes required in many applications, result in components that are often difficult and expensive to manufacture (1).

Formability of sheet has been extensively studied for automotive-type applications which utilize ferritic steels (2,3). A review of aerospace parts reveals that although the names of the products are different, from what is encountered in automotive applications, the inherent issues associated with sheet forming remain the same. Therefore, the same level of understanding that has been obtained in the automotive industry is required if the aerospace industry is to ensure quality, cost-effective sheet products. Most of the forming work performed on superalloys is at elevated temperature to reduce forming loads. The focus of this research is an examination of the metallurgical factors that affect the room-temperature sheet formability of several nickel-based superalloys. Ideally, this project will lead to a better understanding that allows these materials to be formed at room temperature; resulting in a significant cost savings.

The formability of sheet product is normally measured by the forming limit diagram (FLD) (3). Originally when the first FLD's were developed, it was assumed that the curve shape for low carbon steels would be universally applicable to all ductile materials. Since that time it has, however, come to be understood that each material may possess a unique curve.

The forming limit diagram (3) represents the acceptable limits of strain in surface-strain space, where the material does not form a neck or fracture (see Figure 1). The forming limit diagram is constructed by first applying a grid of circles to an undeformed piece of sheet metal. The sheet is cut into varying widths and then deformed. The deformation of the sheet is stopped after the formation of a localized neck. Circles near the neck are then classed into three types: safe, necked and failed. The definition of a failed circle is a circle where deformation has proceeded to the point of fracture. The major and minor axes of the deformed circles are measured, converted to strains and plotted on a surface-strain space graph. A line is then constructed which separates the safe circle data points from the necked and failed data points. Any combination of surface strain which exceeds the forming limit curve will result in the formation of a localized neck or fracture. Formation of a localized neck is a rejection condition in most sheet-metal forming operations and thus is to be avoided. Ideally, during development of a new stamped part the diagram will be used to determine whether there are locations within the part that are near the end of useful deformation. The forming limit diagram is divided into two halves, the left-hand side is the drawing side (negative minor strain) and the right-hand side is the stretching side (positive minor strain). The point on the forming limit curve where the minor strain is zero is referred to as the plane-strain forming limit or FLD_0 . This point often is the minimum point on the diagram.

Effects of Mechanical Properties on FLD

The shape of the forming limit diagram is a function of the thickness of the material being formed and the mechanical properties of the material. The primary mechanical property that affects the FLD is the work-hardening rate of the material. The plastic anisotropy as measured

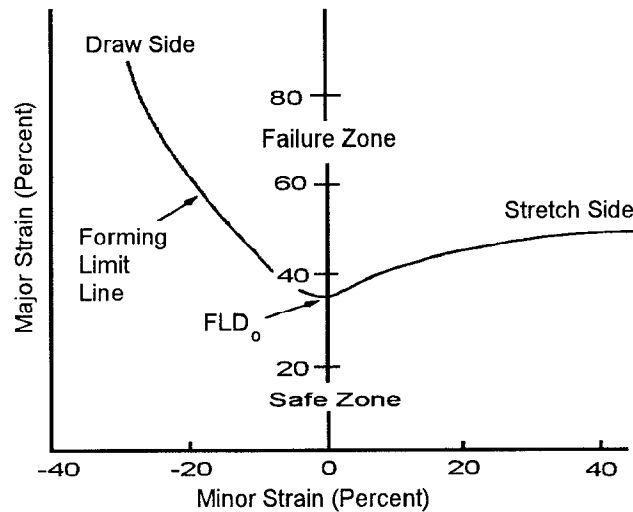


Figure 1. Standard out-of-plane forming limit diagram showing the forming limit line and both safe and failure regions (adapted from reference 3).

by the r -value and yield stress are mechanical properties which influence formability but do not directly affect the FLD. In metal-forming operations the strain rate and temperature can also influence the mechanical properties of the work piece.

The location of the plane-strain forming limit (FLD_0) has been shown to increase in carbon steel with the thickness of the material tested. The functionality of FLD_0 with thickness has been related to the appearance of the localized neck as sheet thickness increases (4).

The most important mechanical property influencing the cold forming of sheet is the work hardening rate (5). One quantitative measure of the work-hardening rate is the strain-hardening exponent, n . A high work-hardening rate enhances the formability of a sheet by allowing an area which thins prematurely to harden and thus become stronger than the surrounding material. The increase in strength in the thin region will allow the deformation to pass to the surrounding material. In this fashion the entire sheet will contribute to deformation. The process of deformation will continue in this manner while there is a balance between the rate of hardening and the rate of thinning. Once the thinning rate is larger than the work-hardening rate, a localized strain will occur which leads to the eventual local failure of the sheet. Since the work hardening rate increases the maximum acceptable deformation that material can withstand, any microstructural feature that increases the work hardening rate usually increases formability. Recrystallization structures produce low yield strengths and high work hardening rates. Low stacking fault energy also increases the work hardening rate.

The plastic-strain ratio (r -value) is the ratio of the thickness strain to the width strain during uniaxial stretching. The normal (\bar{r}) and planar anisotropy (Δr) values are based on the average of the plastic strain ratio determined at three orientations in the sheet (longitudinal (0°), diagonal

(45°), transverse (90°)). For an isotropic material \bar{r} equals 1.0 and Δr equals 0.0 (6). Normal anisotropy is considered to have a good value when numbers are significantly in excess of 1.0. Physically a value in excess of 1.0 means that the sheet is able to resist deformation in the through thickness direction. Planar anisotropy is not related to the thinning resistance, it is related to the ability of a sheet to resist earing. Higher values of normal anisotropy have a significant effect on the strain path of a material on the drawing side but little if any effect on the stretch side of the forming limit diagram. On the draw side, higher \bar{r} values cause the strain path to intersect the forming limit curve at higher values of major strain (3).

Alloys Studied

In this study the following alloys were examined.

Alloy 625LCF. Alloy 625 has excellent weldability characteristics and is considered to be one of the most weldable superalloys (7). The corrosion resistance of Alloy 625 is also excellent. Alloy 625 has found wide use in aerospace applications and in marine usage. Many derivatives of Alloy 625 have been made over the years since this alloy was initially developed and it is one of these derivatives that will be the focus of this study. Alloy 625LCF was developed to improve the intermediate temperature low cycle fatigue properties of Alloy 625. Alloy 625 does not precipitate γ' but does precipitate γ'' which has a BCT structure. To accomplish improved low cycle fatigue performance, modifications were made to limit the amount of carbon, nitrogen and silicon (8). Grain size is also reduced in this modified alloy which further enhances its properties.

Alloy 718. Alloy 718 is readily fabricated by both conventional forming and welding. Alloy 718 has found extensive use in aerospace applications as well as land-based gas turbine applications (9). Alloy 718 is an austenitic nickel-based alloy which is used in applications requiring high strength to 760°C (1400°F) and oxidation resistance to 982°C (1800°F). Alloy 718 is a precipitation hardenable alloy. The major strengthening phases are γ' and γ'' . γ'' is the main strengthening phase and has a DO₂₂ BCT crystal structure. For this study Alloy 718 was used in the solution-annealed condition. Thus, there should be no γ'' or γ' . There will however be δ remaining as well as various carbides. In the solution annealed condition at low strains dislocations move in planar arrays (10). The planar motion of dislocations would equate to a high work-hardening rate at low strains.

Alloy 718SPF. Alloy 718SPF (SPF is the designation for super plastic forming) is a derivative of Alloy 718 and as such has much of the same physical metallurgy as Alloy 718. Alloy 718SPF has processing differences which are designed to aid in the control of grain size during the high temperature superplastic forming process. Alloy 718SPF also has chemistry restrictions that are tighter than the standard specifications for Alloy 718. The elements that have tighter controls are: Nb, C, S and N. Alloy 718SPF is sold under the same specifications as Alloy 718.

Experimental Procedure

Experimental samples in the form of 0.50 mm (0.020 in) thick commercially cold rolled and annealed sheets of Alloy 625LCF, 718, and 718SPF were received for analysis. The compositions of the experimental alloys are summarized in Table I. All compositions met accepted specifications for the individual alloys.

TABLE I - Chemical Compositions of Alloys 625LCF, 718 and 718SPF (weight percent)

Nominal Compositions of Alloys 625LCF, 718, and 718SPF									
Alloy	Ni	Cr	Fe	Mo	Nb+Ta	Ti	Al	C	N
625LCF	62.0	20.7	2.5	9.0	3.7	0.2	0.1	0.021	0.020
718	52.5	19.0	19.0	3.1	5.0	1.0	0.5	0.047	0.006
718SPF	52.5	19.0	19.0	3.1	4.9	1.0	0.6	0.022	0.006

Mechanical properties were obtained with standard E-8 tensile samples with a longitudinal orientation with respect to the rolling direction. These specimens were tested at room temperature at strain rate of $0.0024s^{-1}$.

Table II shows the sample types that were used for determination of the FLD. The Type I, III, and IV are geometries described by Raghavan (4). Each of the Raghavan samples was 177.8 (7.0 in) long by 177.8 mm (7.0 in) initial width. Type I and III geometries have a semicircular cutout on each side of the sample, leaving an effective width across the center region. Type IV geometry is rectangular or square. The hourglass sample is similar to Type I but the initial width is less than 177.8 mm (7.0 in). The smaller initial width produces a more severe gradient in geometry but requires less material. The hourglass samples were only used for Alloy 718SPF due to the limited amount of available material. Grids of 2.54 mm (0.10 in) diameter circles were electro-etched on all samples prior to testing. Samples were deformed on a limiting dome height (LDH) system adapted to a commercial servohydraulic test system equipped with a 101mm (4.0 in) diameter ball at various load rates which produced an approximate displacement rate of 12.7 mm/min (0.5 in/min). Four sheets of 0.076 mm (0.003 in) polyethylene were used to provide a fully lubricated condition. A specialized technique which sensed an error signal change with the load drop associated with neck formation was used to stop the test (11).

TABLE II - Sample Types Used for Out-of-Plane Forming Limit Tests

Effective Width, mm (in.)	Sample Type
25.4 (1.0)	I or Hourglass
38.1 (1.5)	I or Hourglass
50.8 (2.0)	I or Hourglass
63.5 (2.5)	I or Hourglass
76.2 (3.0)	I or Hourglass
127.0 (5.0)	III
133.4 (5.3)	III
139.7 (5.5)	III
152.4 (6.0)	IV
177.8 (7.0)	IV

Deformed circles were measured with an optical image analysis system. Measurements of the longest axis and smallest axis of each circle were used to determine the major strain and minor strain. Circles which did not have a necked region or a crack were classified as safe. Circles with either a necked region or crack were so labeled. Plots of major strain versus minor strain for all the measured circles for each alloy were produced. The forming limit curve was drawn on each plot by assuring that all necked and failed points were above the curve.

Results

All of the forming limit curves presented in this section have several lines drawn on them to represent different strain paths to aid in interpretation of the figures. The strain path is often represented by the value of β which is the ratio of the minor true strain to the major true strain. The left most line on the figures represents the tension line corrected to the plastic-strain ratio determined in uniaxial testing. The next line represents the $\beta=-0.5$ strain path or uniaxial tension for an isotropic material. The line that passes through a minor strain of 0.0 represents a strain path of $\beta=0.0$ or plane strain. The line furthest to the right represents a $\beta=1.0$ strain path or biaxial stretching.

Figures 2, 3 and 4 show the out-of-plane limiting strain ratios for Alloy 625LCF, 718 and 718SPF respectively. For each of these figures numerous safe points were measured but are not presented to minimize clutter. The forming limit curves for each alloy were drawn below all necked as well as all failed data points. The data to the left of plane strain contain a large number of necked data points indicating the ability to stop the testing at the onset of necking. To the right of plane strain only a few necked points are indicated. The lack of necked data points indicates the limits of sensitivity available using the experimental method. The necked data points exhibited in these figures were taken from necks that were evident at a position diametrically opposed to the location of the crack as would be expected from the literature (12,13). The necked and failed regions do not show a clean demarcation from each other. This lack of separation is related to normal scatter in the material properties and the experimental technique. The low point of the limiting strains appears to be to the right of plane strain for these alloys.

Discussion

Comparison of Alloys

The basic mechanical properties for the alloys in this study are summarized in Table III (11). Alloys 625LCF and 718SPF have very similar mechanical properties in the solution annealed conditioned that was used for the present study. Alloy 718 has slightly lower strengths and slightly higher strain-hardening exponent, as compared to the other two alloys. All three alloys have similar strain rate sensitivities, m , and they are fairly isotropic since \bar{r} is close to the 1.0 for all three alloys. Figure 5 shows the out-of-plane forming limit diagrams for all three alloys on a single plot. The general forming limit diagram shapes are in agreement with what is observed for other alloys. The order of the alloys on the left side from best to worst is Alloy 718, 625LCF, 718SPF with very little separation between the alloys. The order on the left side of the FLD often follows the materials ductility as measured by the uniaxial tension total

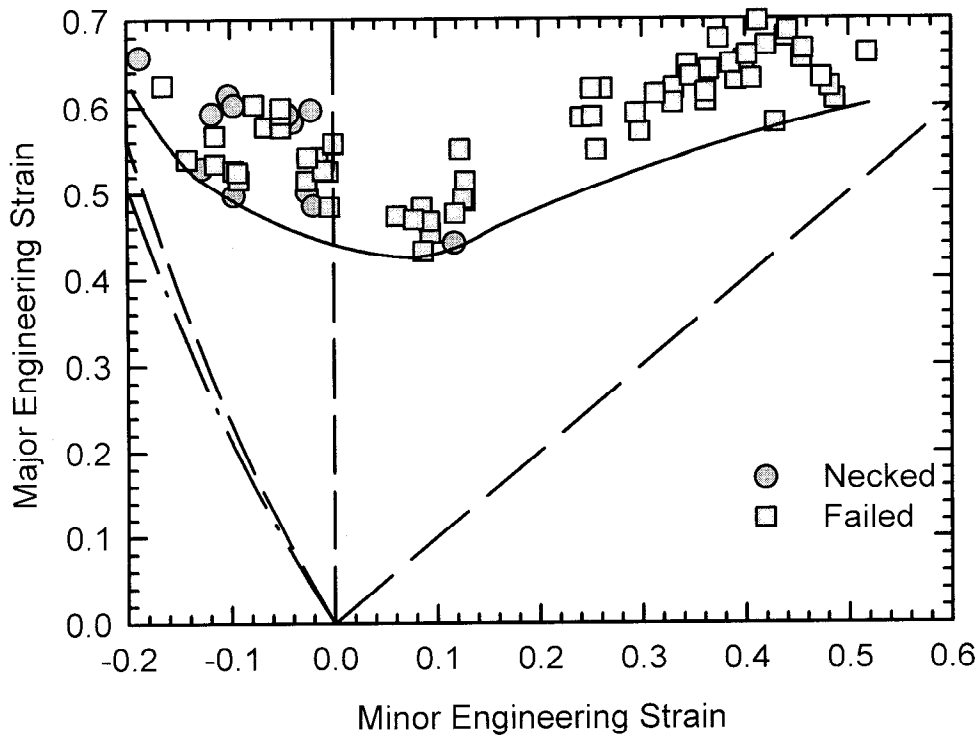


Figure 2. Out-of-plane limiting strain ratios for Alloy 625LCF as determined from specimens tested at room temperature in a longitudinal orientation.

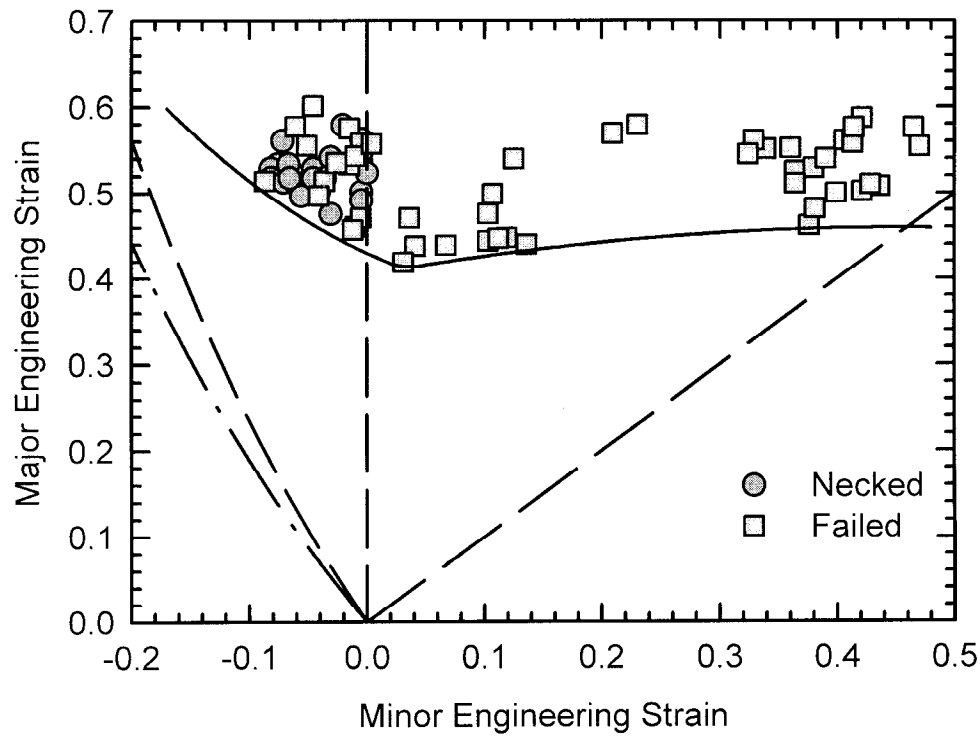


Figure 3. Out-of-plane limiting strain ratios for Alloy 718 as determined from specimens tested at room temperature in a longitudinal orientation.

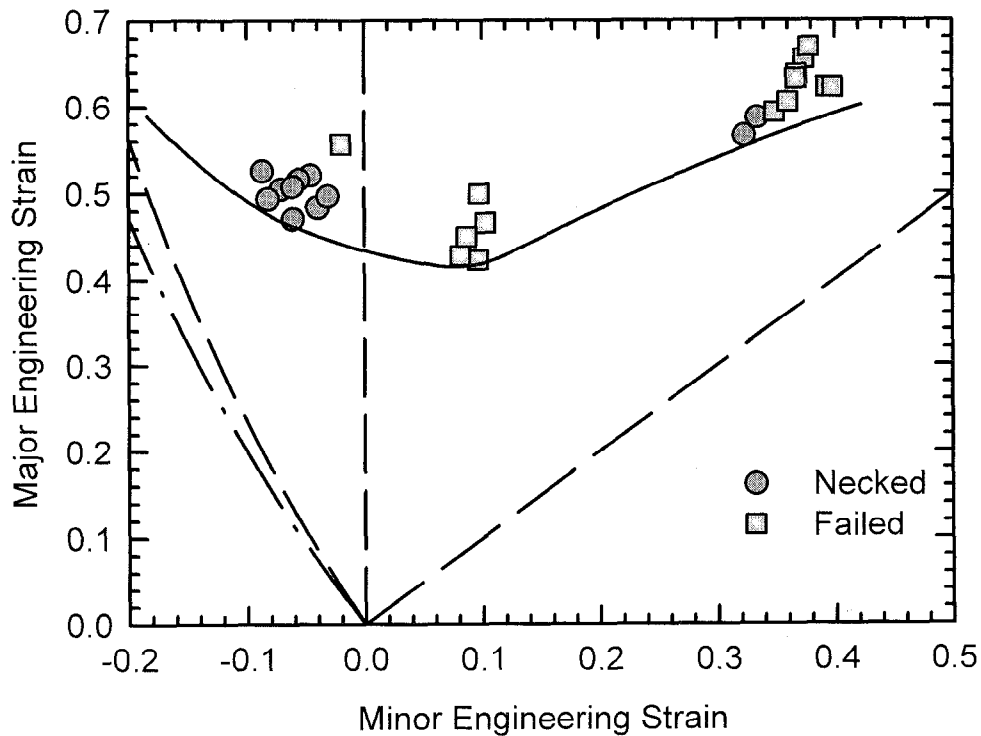


Figure 4. Out-of-plane limiting strain ratios for Alloy 718SPF as determined from specimens tested at room temperature in a longitudinal orientation.

TABLE III - Basic Ambient Temperature Mechanical Properties from a Longitudinal Orientation at a Strain Rate of 0.0024 s^{-1} (11).

Alloy	Yield Strength, MPa (ksi)	Ultimate Tensile Strength, MPa (ksi)	n	m*	\bar{r}	Elongation, %
625LCF	524 (76.0)	974 (141.2)	0.42	0.0025	0.97	42.0
718	471 (68.3)	945 (137.1)	0.44	0.0025	0.92	39.3
718SPF	536 (77.7)	995 (144.3)	0.41	0.0029	1.06	39.5

*m values were determined at 30% engineering strain over a strain rate range of 0.000024 s^{-1} to 0.24 s^{-1}

elongation. As seen in Table III, the total elongation is similar for the three alloys. The three alloys also group together at the plane-strain intercept which agrees with their similar values of strain-hardening exponent.

The right-hand side of the FLD shows that Alloy 718SPF and 625LCF have the best biaxial stretching behavior. Alloy 718 however shows lesser performance on the right side of the FLD. The difference in behavior between Alloy 718SPF and 718 is particularly intriguing because these alloys perform somewhat similarly in uniaxial tension.

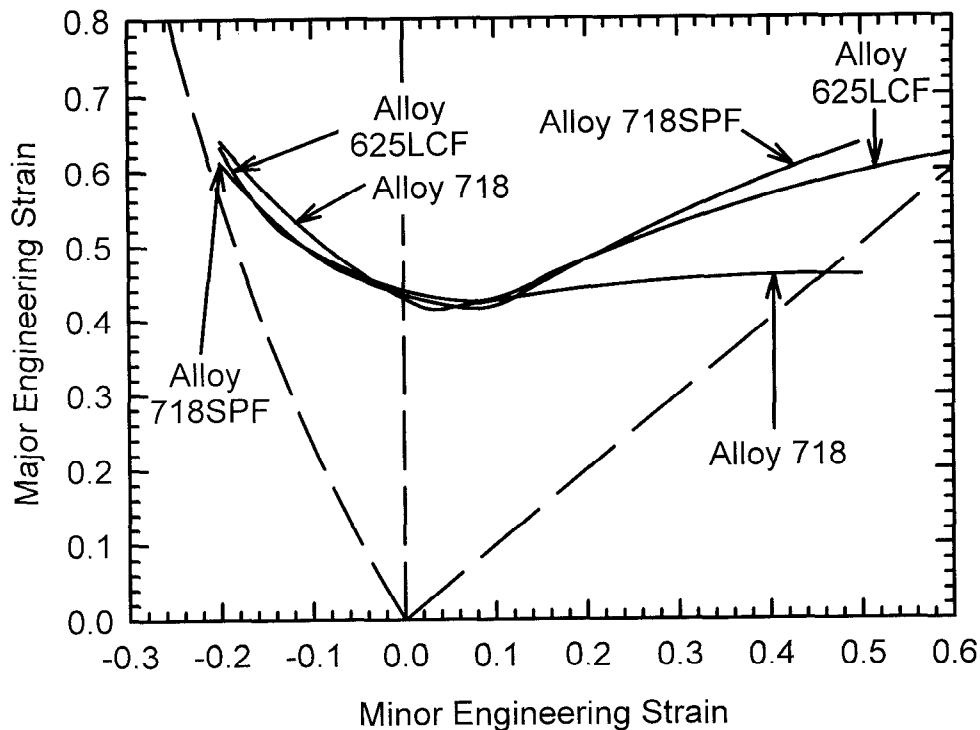


Figure 5. Combined room temperature out-of-plane forming limit curves for Alloys 625LCF, 718, and 718SPF.

The equivalence of performance of Alloys 718 and 718SPF at plane strain and the left-hand side of the FLD is in contrast to the lower performance of Alloy 718 on the right-hand side of the FLD. The lack of correspondence on the stretch side of the FLD (right-hand side) between Alloys 718 and 718SPF clearly indicate that the controlling factor(s) on the stretch side of the forming limit diagram are different from those at plane strain and on the draw side. The stretch side of the forming limit diagram must then be controlled by different microstructural features than the draw side of the forming limit diagram. In other studies it has been found that the stretch side of the forming limit diagram is controlled by the failure or fracture mode of the alloys (14).

Termination of straining on the right-hand side was considered by Marciniak and Kuczynski (15). Marciniak and Kuczynski proposed a theory which assumes that failure begins at a material inhomogeneity. These inhomogeneities produce a condition which will allow the formation of a localized neck and subsequently fracture. To account for these inhomogeneities mathematically, an f factor was defined. Marciniak and Kuczynski showed that as the f factor decreases the forming limit on the right side of the diagram occurs at lower values of major strain. The nature of the inhomogeneity was postulated to be representative of naturally occurring nonhomogeneous thicknesses or material properties (14). The inhomogeneities also could be considered to be inclusions. From the work of Yuki it is known that as volume fraction of inclusions increases the biaxial stretching limiting strains decrease (16). The work of Yuki also shows that at plane strain and uniaxial tension forming limits are not affected as significantly by inclusions. At plane strain and in uniaxial tension the controlling factor was shown to be the matrix properties. The data obtained in this project are consistent with Yuki's observation.

Alloy 625LCF and 718SPF support the correlation of biaxial limiting strain with volume fraction of inclusions. Both alloys are refinements of the base alloy. The refinements include chemistry changes reduce the levels of interstitial elements (see Table I). Figures 6 and 7 show that fracture surfaces for the biaxial stretched specimens of Alloys 625LCF and 718SPF. These micrographs show the presence of many small dimples and a limited number of larger voids due to the limit number of large inclusions.

In contrast to Alloy 625LCF and 718SPF, Alloy 718 shows many large inclusions on the fracture surface of the biaxially stretched specimen. Figure 8 shows large inclusions and flat spots around the particles. The flat regions show shallow elongated dimples which are indicative of shear stress induced deformation. This evidence leads to the postulation that failure begins at particles and rapidly proceeds to fracture. The fracture occurs at lower strains than the failure that is seen in Alloy 718SPF which shows no evidence of large flat fracture regions.

A quantitative analysis of the second phase particles that can be observed at 1000X (particles approximately 1 μ m and larger) for Alloys 718 and 718SPF was conducted to verify the fracture surface observations. Samples of each alloy were mounted in three different orientations with respect to the original rolling direction. These samples were ground and polished. A total of 240 fields was examined in each material (*i.e.* 4 specimen/material at 3 orientations with 20 fields for each orientation). Table IV shows the percent second phase that was measured for the two alloys. Table IV clearly indicates that the amount of large second phase particles is greater in Alloy 718 as compared to Alloy 718SPF. There were several qualitative observations that were seen during the particle characterization. Both alloys have many small spherical particles (less than 2 μ m in diameter). Both alloys had a few large blocky particles (2 to 10 μ m in size and elongated). There were more large particles present in Alloy 718 as compared to Alloy 718SPF. The distribution of the particles in both alloys was very non-uniform with the larger particles frequently appearing in bands.

TABLE IV - Analysis of Particle Phase Fractions in Alloy 718 and 718SPF

Alloy	Percent Second Phase Particles	
	718	718SPF
L*	1.6 \pm 0.8	0.8 \pm 0.7
T	1.5 \pm 0.5	0.8 \pm 0.2
ST	0.9 \pm 0.3	0.7 \pm 0.4
Average	1.4 \pm 0.6	0.8 \pm 0.4

*: Orientation of polished sample with respect to original rolling direction

L: Longitudinal orientation

T: Transverse orientation

ST: Short transverse orientation

Qualitative chemical analysis was performed using electron dispersive spectrometer attached to an SEM on ten particles from each alloy. The analysis showed the presence of Nb, Ti, and often N. Both the large blocky particles and the small spherical particles had the same elements present. The qualitative elemental composition of the particles were similar for both Alloy 718 and Alloy 718SPF.

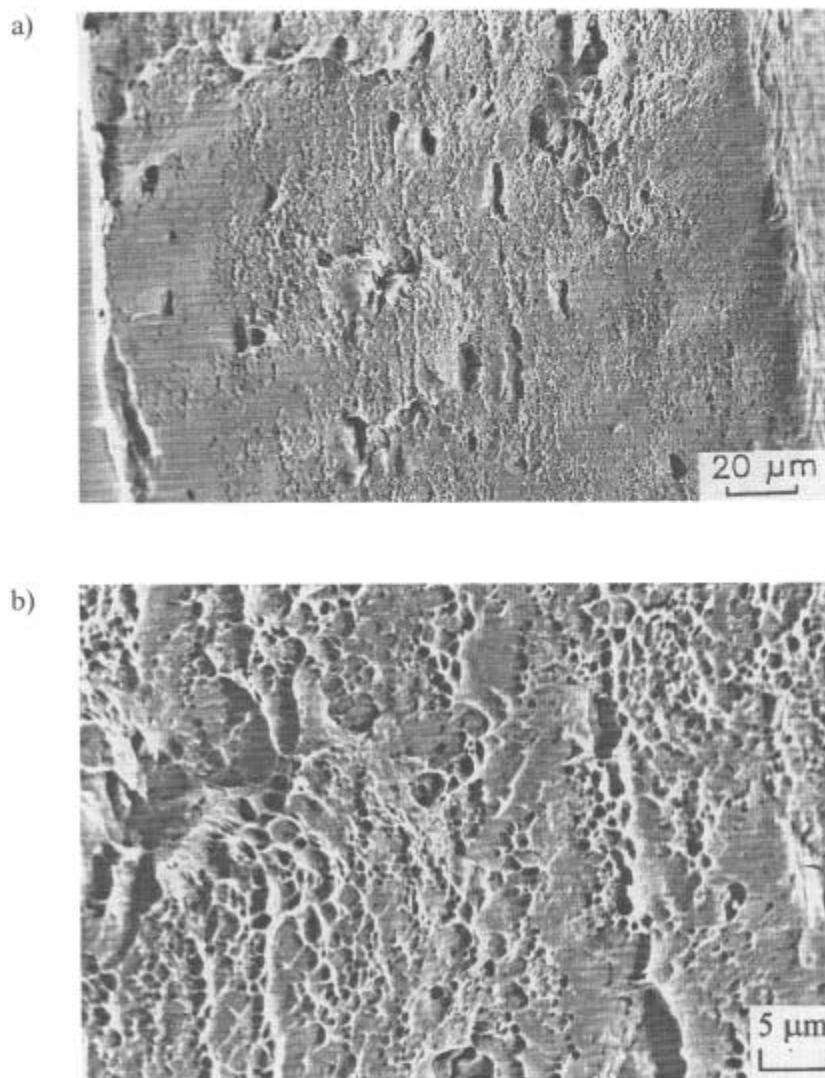


Figure 6. Secondary electron image of Alloy 625LCF fracture surface from a biaxially stretched sample deformed out-of-plane at room temperature. a) Low magnification. b) High magnification.

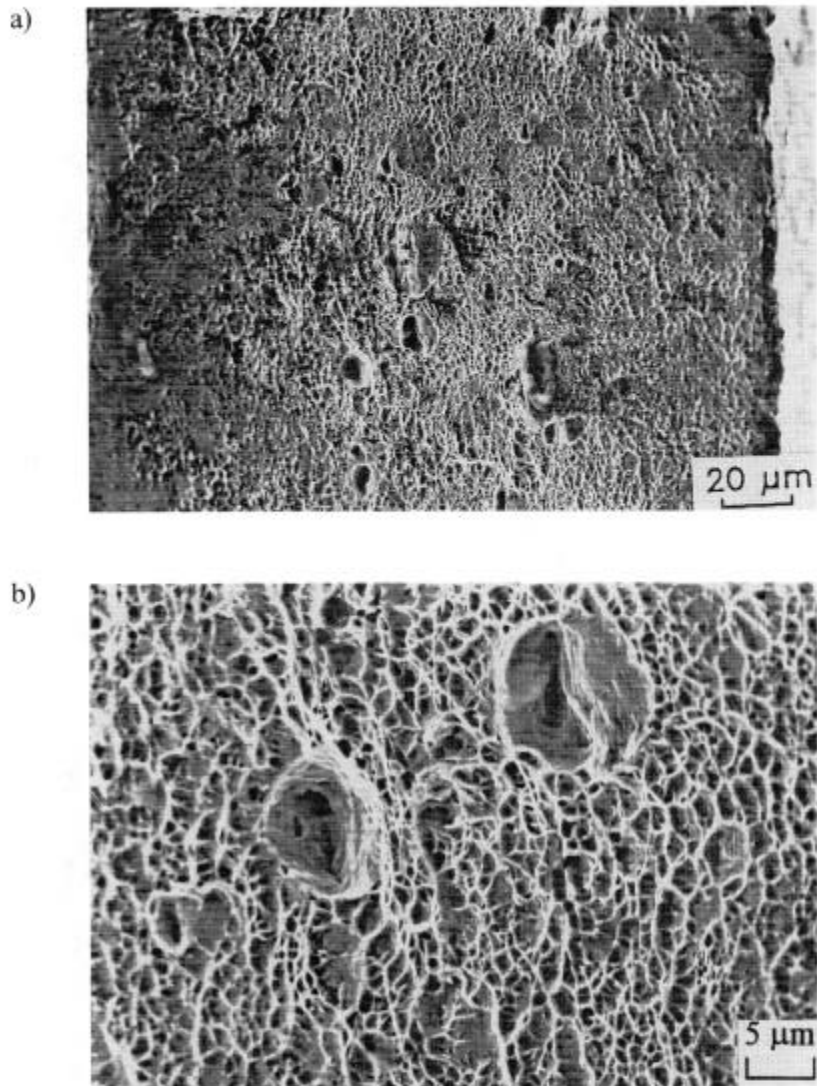


Figure 7. Secondary electron image of Alloy 718 SPF fracture surface from a biaxially stretched sample deformed out-of-plane at room temperature. a) Low magnification. b) High magnification.

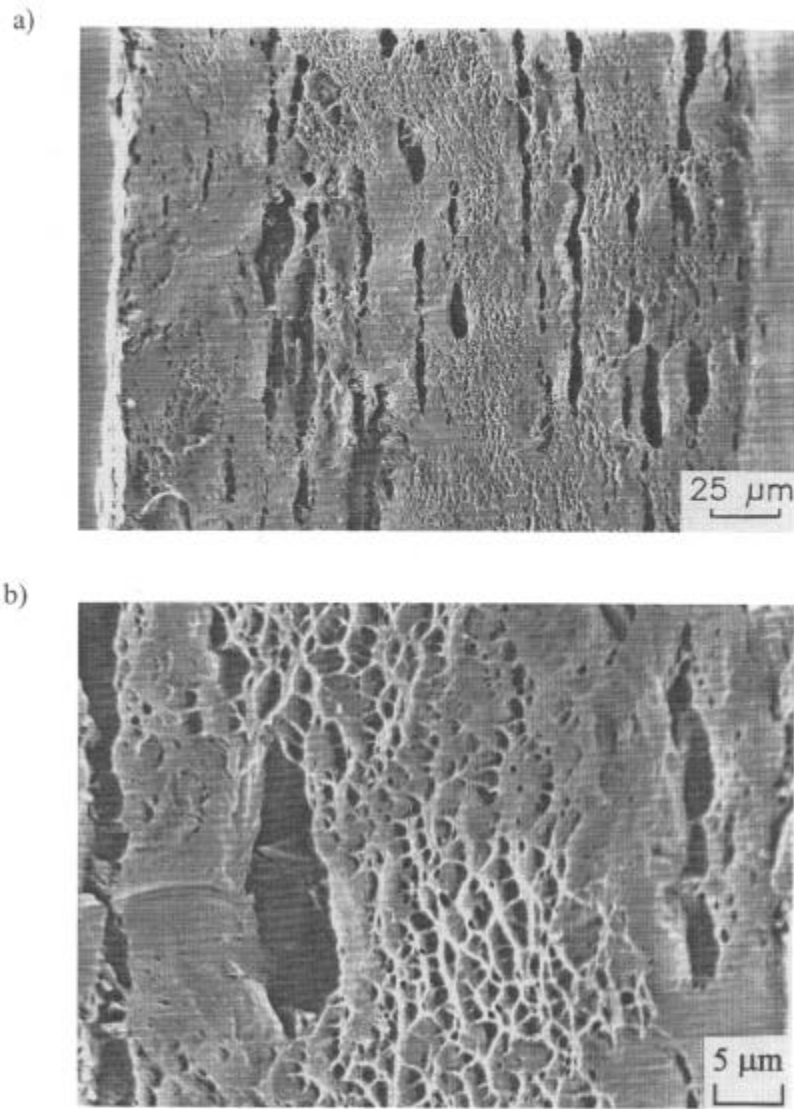


Figure 8. Secondary electron image of Alloy 718 fracture surface from a biaxially stretched sample deformed out-of-plane at room temperature. a) Low magnification. b) High magnification.

Summary

The forming limit curves for Alloys 625LCF, 718 and 718SPF have been presented. All three alloys show similar performance on the draw (left-hand) side of the forming limit diagram and at plane strain. On the stretch (right-hand) side however there is a distinct difference in the forming limit curves for these alloys. The forming limit curve of Alloy 718 is lower due to the increased number of second phase particles, which alters the fracture behavior of this alloy during biaxial stretching.

Acknowledgements

The image analysis work of Mr. J. Johnson, Mr. D. Merchant and Mr. A. Brewer is gratefully acknowledged. This work was supported by the Advanced Steel Processing and Products Research Center at the Colorado School of Mines, an NSF-sponsored Industry/University Cooperative Research Center.

References

1. B. Hicks, "High Temperature Sheet Materials for Gas Turbine Applications", *Materials Science and Technology*, Vol. 3, 1987, pp. 772-781.
2. K.S., Raghavan, R.C. Van Turen and H. Darlington, "Recent Progress in the Development of Forming Limit Curves for Automotive Sheet Steels", SAE Paper #920437, SAE, Dearborn, MI, 1992, pp. 87-104.
3. S.P. Keeler, "Automotive Sheet Metal Formability", Report AU 89-1, Automotive Committee, AISI, Pittsburgh, PA, January 1989, pp. 4.2.1-4.2.15.
4. K.S. Raghavan, "A Simple Technique to Generate In-Plane Forming Limit Curves and Selected Applications", *Metallurgical and Materials Transactions A*, Vol. 26A, 1995, pp. 2075-2084.
5. A.K. Ghosh, S.S. Hecker, and S.P. Keeler, *Workability Testing Techniques*, edited by G.E. Dieter, ASM, Metals Park, OH, 1984, pp. 135-195.
6. Roger Pearce, *Sheet Metal Forming*, Adam Hilger, Bristol, England, 1991, pp. 3-44.
7. S. Floreen, G. E. Fuchs and W. J. Yang, "The Invention and Definition of Alloy 625", in *Superalloys 718, 706, 625 and Various Derivatives*, edited by E.A. Loria, TMS, Warrendale, PA, 1994, pp. 13-37.
8. D.E. Jordan, "Welding of High Molybdenum Nickel Base Alloys", preprint, paper to be published.
9. M.J. Weis, "The Hot Deformation Behavior of As-Cast Alloy 718", M.S. Thesis T-3382, Colorado School of Mines, Golden, CO, 1987.

10. M. Sundaraman, P. Mukhopadhyay and S. Banerjee, "Precipitation and Room Temperature Deformation Behavior of Inconel 718", in *Superalloys 718, 706, 625 and Various Derivatives*, edited by E.A. Loria, TMS, Warrendale, PA, 1994, pp. 419-440.
11. P. Roamer, "Formability of Nickel-Based Alloy Sheet at Room Temperature", M.S. Thesis, Colorado School of Mines, Golden, CO, 1997.
12. A.K. Ghosh and S. S. Hecker, "Failure in Thin Sheets Stretched Over Rigid Punches", *Metallurgical Transactions A*, Vol. 6A, 1975, pp. 1065-1074.
13. M. Azrin and W. A. Backofen, "The Deformation and Failure of a Biaxially Stretched Sheet", *Metallurgical Transactions*, Vol. 1, 1970, pp. 2857-2865.
14. Roger Pearce, *Sheet Metal Forming*, Adam Hilger, Bristol, England, 1991, pp. 159-173.
15. Z. Marciniak and K. Kuczynski, "Limit Strains in the Process of Stretch-Forming Sheet Metal", *International Journal of Mechanical Sciences*, Vol. 9, 1967, pp. 609-620.
16. N. Yuki, "The Effects of Matrix Constitutive Behavior and Inclusions on Ductility and Ductile Fracture of Fe-42 pct Ni Alloy", M.S. Thesis T-4773, Colorado School of Mines, Golden, CO, 1995.